Geotech Geol Eng (2022) 40:3913–3928
https://doi.org/10.1007/s10706-022-02117-6

TECHNICAL NOTE

# Bearing Capacity of Ring Foundations on Anisotropic and Heterogenous Clays: FEA, NGI-ADP, and MARS

**Van Qui Lai · Jim Shiau · Suraparb Keawsawasvong · Duy Tan Tran**

Received: 8 February 2022 / Accepted: 12 March 2022 / Published online: 9 April 2022


**Abstract** Axisymmetric solutions for the bearing capacity of ring foundation resting on anisotropic and heterogenous clays are presented in this paper using finite element analysis (FEA). The NGI-ADP model in PLAXIS FEA, a widely used anisotropic soil model, is adopted to study the stability responses of ring foundations, with special consideration given to the effects of increasing undrained shear strength with the depth. Numerical results are formulated in terms of a dimensionless stability number (bearing capacity ratio) that is a function of three dimensionless input parameters: namely, the ratio of inner and outer radius, the increasing strength gradient ratio, and the anisotropic shear strength ratio. The influence of each dimensionless input parameter on the bearing capacity ratio is investigated using design charts and failure mechanisms, and they are scored by relative importance indexes in multivariate adaptive regression splines (MARS) model—a machine learning approach. A highly accurate equation generated from the MARS model is proposed as an effective tool for engineering practitioners.

**Keywords** Ring foundation · Anisotropic · NGI-ADP model · MARS model · Bearing capacity factor

V. Q. Lai · D. T. Tran
Faculty of Civil Engineering, Ho Chi Minh City University of Technology (HCMUT), 268 Ly Thuong Kiet Street, District 10, Ho Chi Minh City, Vietnam
e-mail: lvqui@hcmut.edu.vn

D. T. Tran
e-mail: tdtan.sdh19@hcmut.edu.vn

V. Q. Lai · D. T. Tran
Vietnam National University Ho Chi Minh City (VNU-HCM), Linh Trung Ward, Thu Duc District, Ho Chi Minh City, Vietnam

J. Shiau
School of Civil Engineering and Surveying, University of Southern Queensland, Toowoomba, QLD, Australia
e-mail: jim.shiau@usq.edu.au

S. Keawsawasvong (✉)
Department of Civil Engineering, Thammasat School of Engineering, Thammasat University, Pathumthani 12120, Thailand
e-mail: ksurapar@engr.tu.ac.th

## 1 Introduction

The use of shallow circular and spudcan footings were popular in the past few decades in supporting axisymmetric structures such as transmission towers, water towers, annular platforms, silos, storage tanks, and chimneys. Nowadays, the more economical ring foundations are often being considered, with the increasing numbers of recent research in this direction.

Several experimental studies were reported in relation to the performance of ring footing in sand (e.g., Ohri et al. 1997; Hataf and Razav 2003) as well as in clay (e.g., Demir et al. 2012; Shalaby 2017). Calculation approaches have been constantly developed,

especially in the area of numerical simulation. For instance, Zhao and Wang (2008) performed the bearing capacity of ring foundations in sandy soil using FLAC; whilst Benmebarek et al. (2012) adopted FLAC and Chavda and Dodagoudar (2019) to estimate $N_c$, $N_q$, $N_\gamma$ considering the effects of the dilation angle, smooth and rough ring footings. Choobbasti et al. (2010) assessed the bearing capacity and settlement of ring footings on homogeneous soils using the finite element analysis. Kumar and Chakraborty (2015) adopted the finite element limit analysis (FELA), Chavda and Dodagoudar (2021) applied FEA, and Gholami and Hosseininia (2017) used method of characteristics to estimate the bearing capacity factors for ring foundations on cohesive-frictional soils. The bearing capacity solution of a ring footing rest on clay was also investigated in Lee et al. (2016), Benmebarek et al. (2017), Khatri and Kumar (2009), Yang et al. (2020), Birid and Choudhury (2021), Keawsawasvong and Lai (2021), and Papadopoulou and Gazetas (2020). Recently, the bearing capacity of a ring foundation on rock mass was studied by Yodsomjai et al. (2021a).

It was generally recognized that undrained shear strength of soils not only increases with depth but also it is directly dependent on the orientation of the major principal stress to the vertical axis or depositional direction (see e.g., Ladd and Degroot 2003; Ladd 1991; Yu and Sloan 1994). In other words, the undrained shear strength of clay exhibits somewhat anisotropic behavior in nature. Recently, some failure criteria were proposed to consider the complex inherent of anisotropic clay such as the Anisotropic Undrained Shear (AUS) model in Krabbenhoft et al. (2019). In addition, the NGI-ADP constitutive model was presented by Grimstad et al. (2012). Although the recent finite element limit analysis is considered as a powerful technique to solve various stability problems in the geotechnical engineering field (e.g., Ukritchon et al. 2019, 2020; Shiau and Al-Asadi 2020a, b, c, d; Shiau and Al-Asadi 2021; Shiau et al. 2021; Keawsawasvong et al., 2022; Keawsawasvong and Ukritchon, 2017a, 2020, 2021; Lai et al. 2021a; Yodsomjai et al. 2021b, c; Beygi et al. 2020; Ukritchon and Keawsawasvong, 2017, 2019, 2020; Tho et al. 2014; Bhattacharya and Sahoo 2017; Bhattacharya 2016, 2018), the displacement-based finite element analysis is also useful in solving the complex boundary conditions (e.g. Shiau and Yu 2000; Shiau and Smith 2006; Shiau et al. 2006a; b, 2018; Shiau and Watson 2008; Halder and Manna 2020; Pirastehfar et al. 2020; Chakraborty and Goswami, 2021; Chatterjee and Murali Krishna 2021; Keawsawasvong and Ukritchon, 2017b; Hamouma et al. 2021; Huynh et al. 2022a, b; Ukritchon et al. 2017a, b).

The application of the NGI-ADP model has been used to analyze several geotechnical problems such as in Zhang et al. (2021), Li et al. (2021), and Langford et al. (2021) for the deep excavation problem; Li and Zhang (2020) for the pile response problem; Aamodt et al. (2021) for the slope stability problem; and Zhang et al. (2020) for the tunnel stability problem. Moreover, the anisotropy effect of soils was investigated for the works related to passive failure modes of plate anchors as well as foundations by Keawsawasvong et al. (2021), Keawsawasvong and Lawongkerd (2021), Nguyen et al. (2021), and Lai et al. (2022). Nevertheless, very few studies were reported in the literature in relation to the bearing capacity of ring footings with the combined effects of clay inhomogeneity and strength anisotropy using the NGI-ADP model.

In this paper, the NGI-ADP model is adopted to investigate the bearing capacity factor and failure mechanism of ring foundations resting on anisotropic and heterogeneous clays. The effects of the three dimensionless input parameters, namely the ratio of the inner to outer radius of the ring foundation, the increasing shear strength gradient ratio, and the anisotropic strength ratio of the cohesive clay on the performance of the ring foundation are investigated. The final outcomes are presented using design tables, charts, and an empirical equation. Due to the complex effect of each parameter on the bearing capacity factor, the multivariate adaptive regression splines (MARS) model is used to examine the sensitivity of each parameter using the output results, as well as to build a correlation equation between the multi-input parameters and output results. The tools provided in this paper would contribute to practical designs of ring footings resting on anisotropic and heterogeneous clays.

## 2 Problem Statement and Numerical Simulation

Shown in Fig. 1 is the problem definition of a rigid ring footing resting on anisotropic and

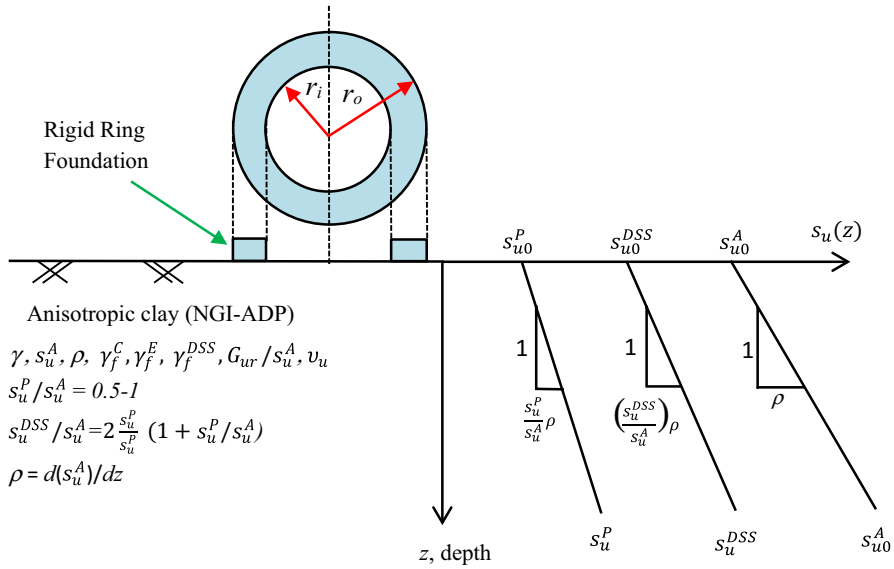


**Fig. 1** Problem definition of a rigid ring footing resting on anisotropic and heterogeneous clay

heterogeneous clay. The soil anisotropy is simulated using the NGI-ADP constitutive model, whilst the heterogeneous clay is studied with the undrained shear strength linearly increasing with depth. The rigid ring footing is subjected to a uniform pressure $q$ and has an external radius $r_o$ and an internal radius $r_i$.

The main soil parameters of the NGI-ADP model are divided into 2 groups: stiffness and strength. The stiffness parameters include $G_{ur}/s_u^A$ (ratio of unloading/reloading shear modulus over the "active" undrained shear strength), $\upsilon_u$ (Poisson's ratio), and $\gamma_f^C, \gamma_f^E, \gamma_f^{DSS}$ (shear strain at failure in triaxial compression, triaxial extension, and direct simple shear respectively). The strength parameters include $s_u^A$ (active undrained shear strength), $s_u^P$ (passive undrained shear strength), and $s_u^{DSS}$ (direct simple undrained shear strength). Accordingly, the strength ratios required in the program input are $s_u^P/s_u^A$, $s_u^{DSS}/s_u^A$, $_0/s_u^A$ (initial mobilization), $s_u^{C,TX}/s_u^A$ (ratio of triaxial compressive shear strength over active shear strength), and the soil unit weight $\gamma$. The ratio of direct simple shear strength over the active shear strength, i.e., $s_u^{DSS}/s_u^A = \frac{2s_u^P}{s_u^A}/\left(1 + s_u^P/s_u^A\right)$, is assumed to be a harmonic mean (Krabbenhoft et al. 2019; Keawsawasvong et al. 2022). Figure 2 shows the failure criterion of the NGI–ADP model in the $\pi$—plane. Detailed descriptions of the model are stated in Grimstad et al. (2012), Ukritchon and Boonyatee (2015) and Brinkgreve and Vermeer (2019) and will not be repeated here.

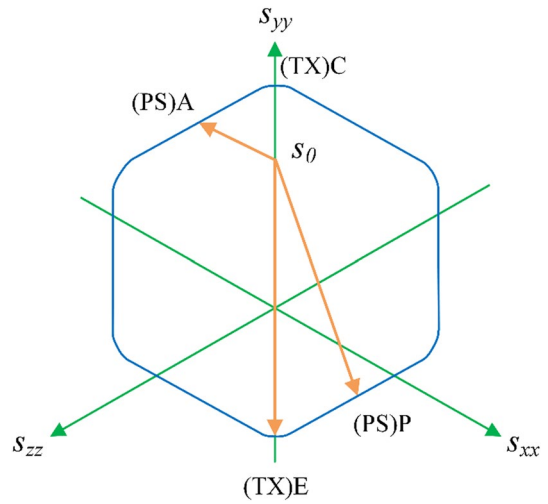


**Fig. 2** Failure criterion of the NGI–ADP model in the $\pi$—plane (After Grimstad et al. 2012)

Following the discussion of the anisotropic soil model, heterogeneous clay is expressed by using the three anisotropic undrained shear strengths that are linearly increasing with depth. They are presented in Eqs. (1)–(3).

$$s_u^A = s_{u0}^A + \rho.z \tag{1}$$

$$s_u^{DSS} = s_{u0}^{DSS} + \frac{s_u^{DSS}}{s_u^A}.\rho.z \tag{2}$$

$$s_u^P = s_{u0}^P + \frac{s_u^P}{s_u^A}.\rho.z \tag{3}$$

where $s_{u0}^A, s_{u0}^{DSS}, s_{u0}^P$ are the anisotropic undrained shear strengths at the ground level, $\rho$ is the linear-gradient with a unit of kPa/m (per meter depth), z indicates the depth determined from the ground surface (see Fig. 1). Note that these undrained shear strengths $s_u^A, s_u^{DSS}, s_u^P$ can be obtained from three modes of shearing, including undrained tests of triaxial compression (for $s_u^A$), triaxial extension (for $s_u^P$), and direct simple shear (for $s_u^{DSS}$). For typical cohesive soils, undrained shearing strength of triaxial compression, $s_u^A$ is the largest, followed by direct simple shear, $s_u^{DSS}$, and triaxial extension, $s_u^P$, which is the lowest.

A dimensionless bearing capacity factor $N$ is defined as the ratio of the uniform pressure $q$ over $s_{u0}^A$, and it is a function of the three dimensionless design parameters, namely the ratio of the inner and outer radii $r_i/r_0$, the strength gradient ratio $m = \rho r_0/s_{u0}^A$, and the anisotropic ratio $r_e = s_u^P/s_u^A$. This is shown in Eq. (4)

$$N = \frac{q}{s_{u0}^A} = \propto f\left(r_i/r_0, m = \rho r_0/s_{u0}^A, s_u^P/s_u^A\right) \tag{4}$$

The finite element model with axial symmetry is adopted to investigate the problem, as shown in Fig. 3, by using Plaxis2D v20 (Brinkgreve and Vermeer 2019). The ring footing is modelled as rigid plates subjecting to a uniform pressure $q$. The soils are simulated by using 15-noded triangular elements with the NGI-ADP soil model. The model size was carefully chosen so that the overall velocity field would not interfere the boundary and the effect on the produced results can be minimized. This is shown in Fig. 3. The bottom boundary is fixed in x, y-directions, the right-hand boundary is fixed only in the x-direction, the left-hand boundary is an axisymmetric line, and the ground surface is free. The ranges of parameters chosen for the study are: (1) $r_i/r_0 =$ 0, 0.25, 0.33, 0.5, and 0.75; (2) $m = \rho r_0/s_{u0}^A = 0$, 1, 2.5, 5, and 15; (3) $s_u^P/s_u^A = 0.4$, 0.5, 0.6, 0.7, 0.8, and 1.0. It is to be noted that $s_u^P/s_u^A = 1$ indicates an isotropic clay. The range of

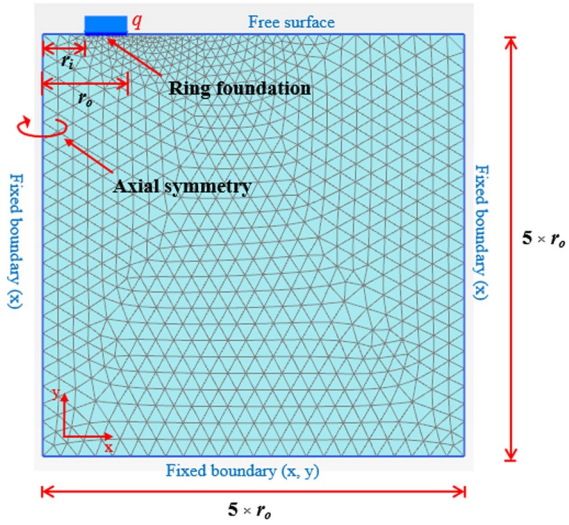


**Fig. 3** Numerical model of a rigid ring footing in axial symmetry (Plaxis 2D)

parameters of $\frac{r_i}{r_0}$ and $m$ was selected based on work of Lee et al. (2016), Benmebarek et al. (2017). According to D'Ignazio et al. (2017) and Hansen and Clough (1981), typical values of $s_u^P/s_u^A$ ratios vary from 0.3 to 0.81. Following the recommendation in the FE Plaxis code, the values of $s_u^{C,TX}/s_u^A = 0.99$, $_0/s_u^A = 0.7$, $\upsilon_u = 0.495$ are adopted for all analyses in the paper. The selected $E_u/s_u^A$ ratio follows a previous stability analysis using FEA (Ukritchon et al. 2017a, b), such that there is very small to none effect of this parameter on the limit load of this stability problem. It should be noted that $_0$ is initial in situ maximum shear stress and $E_u$ is undrained young modulus.

## 3 Validations, Results, and Discussions

To improve the confidence in later parametric analyses, numerical results from finite element analysis (FEA) must be compared with published results (Shiau et al. 2014, 2016a, b, 2017). This is done by comparing with those in Lee et al. (2016) and is presented in Fig. 4 for cases of ring footing on isotropic clay (where the anisotropic ratio $s_u^P/s_u^A = 1$) and heterogeneous clay (the increase shear gradient ratio $m = 0$, 1, 2.5, 5, and 15). The comparison study has shown that the present FEA results of bearing

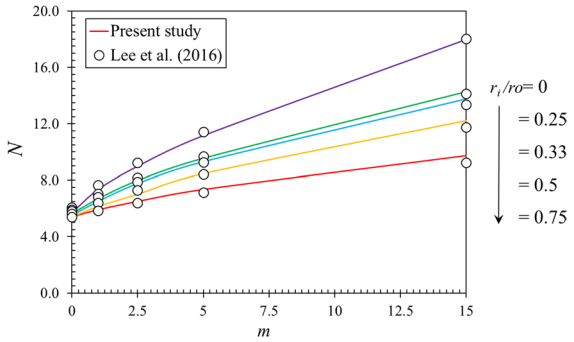


**Fig. 4** Comparison of bearing capacity factor $N$ ~ ring footings on isotropic and heterogeneous clays ($s_u^P/s_u^A=1$)

capacity factor $N$ are in good agreement with those in Lee et al. (2016) and that the current model can be further be used to study the anisotropic effect with reasonable confidence.

With the success of model validation, the next task is to study the effects of the ratio of inner and outer radius ($r_i/r_0$), the anisotropic ratio ($s_u^P/s_u^A$), and the shear strength gradient ratio ($m$) on the bearing capacity factor ($N$). Figure 5 shows the linear relationships of the anisotropic ratio ($s_u^P/s_u^A$) on the bearing capacity factor $N$ for the various cases of $m$ and $r_i/r_o$. Noting that ($s_u^P/s_u^A=1$) indicates an isotropic clay, a decrease in anisotropic ratio ($s_u^P/s_u^A$) means an increased effect of soil anisotropy. For the various $m$ considered in Fig. 5 ($m=0$, 1, 2.5, 15), numerical results have shown that a decrease in ($s_u^P/s_u^A$) results in a decrease in the bearing capacity factor $N$. They have also shown that the bearing capacity factor $N$ decreases with the increasing $r_i/r_0$. Noting that the larger the $r_i/r_0$, the smaller the footing contact area, it is therefore not surprised to see the decreased bearing capacity owing to the reduced footing area (increasing $r_i/r_0$). Besides, it was found that the rate of decrease is more pronounced for larger values of the shear strength gradient ratio $m$.

Using the same results, Fig. 6 shows a nonlinear relationship of the shear strength gradient ratio ($m$) on the bearing capacity factor $N$. The greater the value of $m$, the larger the $N$ is. The rate of increase (the gradient) in $N$ decreases as the ratio of inner and outer radius $r_i/r_o$ increases (less footing area).

The potential failure mechanisms of ring footings in anisotropic and heterogeneous clay are investigated in Figs. 7, 8 and 9. The influence of the anisotropic ratio ($s_u^P/s_u^A$) on the potential failure mechanisms of ring footings is presented in Fig. 7 for the case of ($m=5$ and $r_i/r_o=0.5$). The results of the failure zone and shear band have indicated an unchanged mechanism despite the increase of the ($s_u^P/s_u^A$). It means that the anisotropic ratio ($s_u^P/s_u^A$) has a little effect on the failure mechanism. More specifically speaking, it is true for the undrained clay only where the soil frictional angle is zero. The same observation was made by the recent studies of undrained anisotropic clay in Nguyen et al. (2021) and Keawsawasvong (2021). Despite this, it is not yet to be concluded for drained soils with non-zero frictional angles owing to the lack of published literatures.

A further failure mechanism study on the influence of shear gradient ratio ($m$) is shown in Fig. 8 for the case of ($s_u^P/s_u^A=0.5$ and $r_i/r_o=0.5$). The plots of failure mechanisms have shown that the overall failure zone is reduced in both horizontal and vertical directions as the value of shear strength gradient ratio ($m$) increases. The interference effect (overlapping) of the failure zone diminishes as $m$ increases and the smallest failure zone occurs at the largest value of $m=15$. For the more interesting study, the effects of inner and outer radius ratio ($r_i/r_0$) on the failure mechanism of ring footing are presented in Fig. 9 for the case ($s_u^P/s_u^A=0.5$ and $m=5$). The failure mechanism for a solid circular footing is firstly presented for $r_i/r_0=0$. A ring foundation forms as $r_i/r_0>0$, and the overlapping of failure zone diminishes as the value of $r_i/r_0$ increases, resulting in a Prandtl type of general failure.

## 4 Sensitive Analysis and MARS

The multivariate adaptive regression splines (MARS) model is an automated regression modelling tool. Using several piecewise linear segments (splines) with differing gradients, the relationship between the input variable and output results can be established in multi-dimensions. Recently, the use of the MARS model as the machine learning method in analyzing geotechnical data has become more and more common. Lai et al. (2021a, b) adopted the MARS model to assess the impacts of input design parameters on the output ground movements due to the effects of installing twin caisson foundations. Zhang et al. (2017) proposed an empirical equation to determine

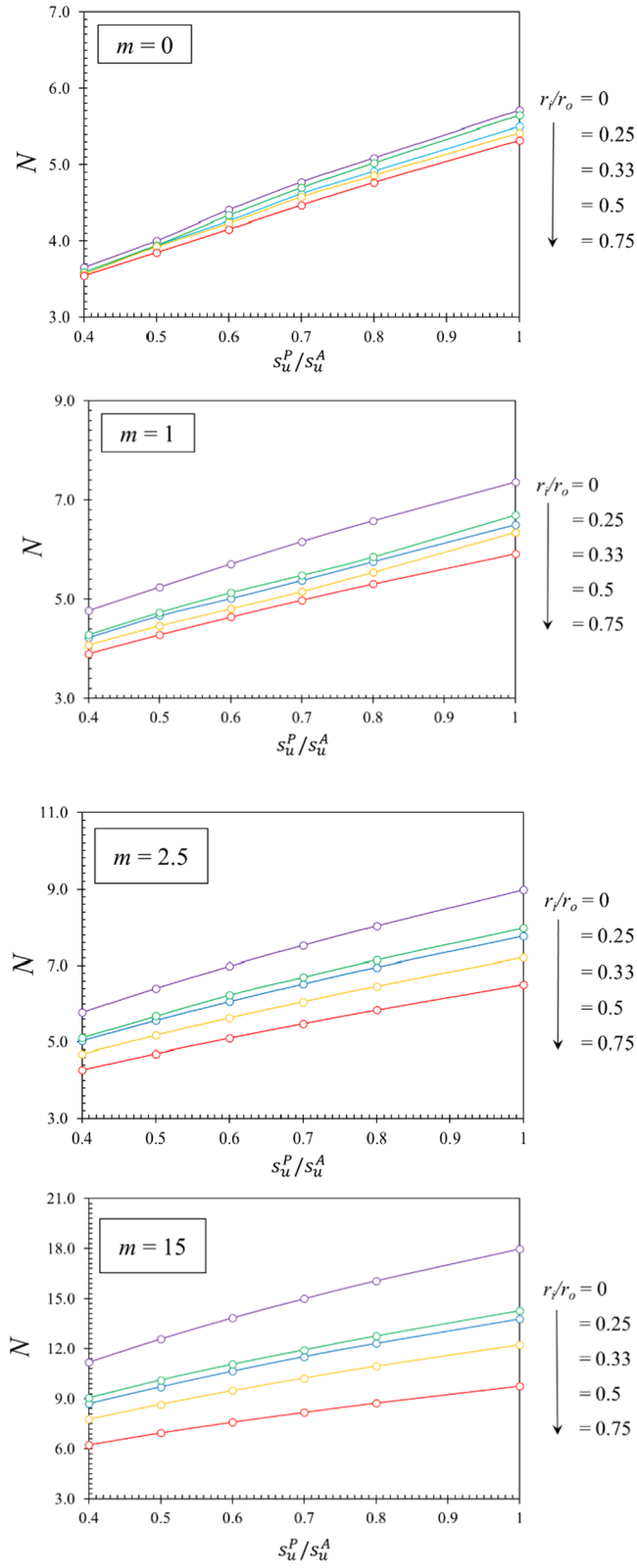


**Fig. 5** Effect of anisotropic ratio ($s_u^P/s_u^A$) on the bearing capacity factor $N$

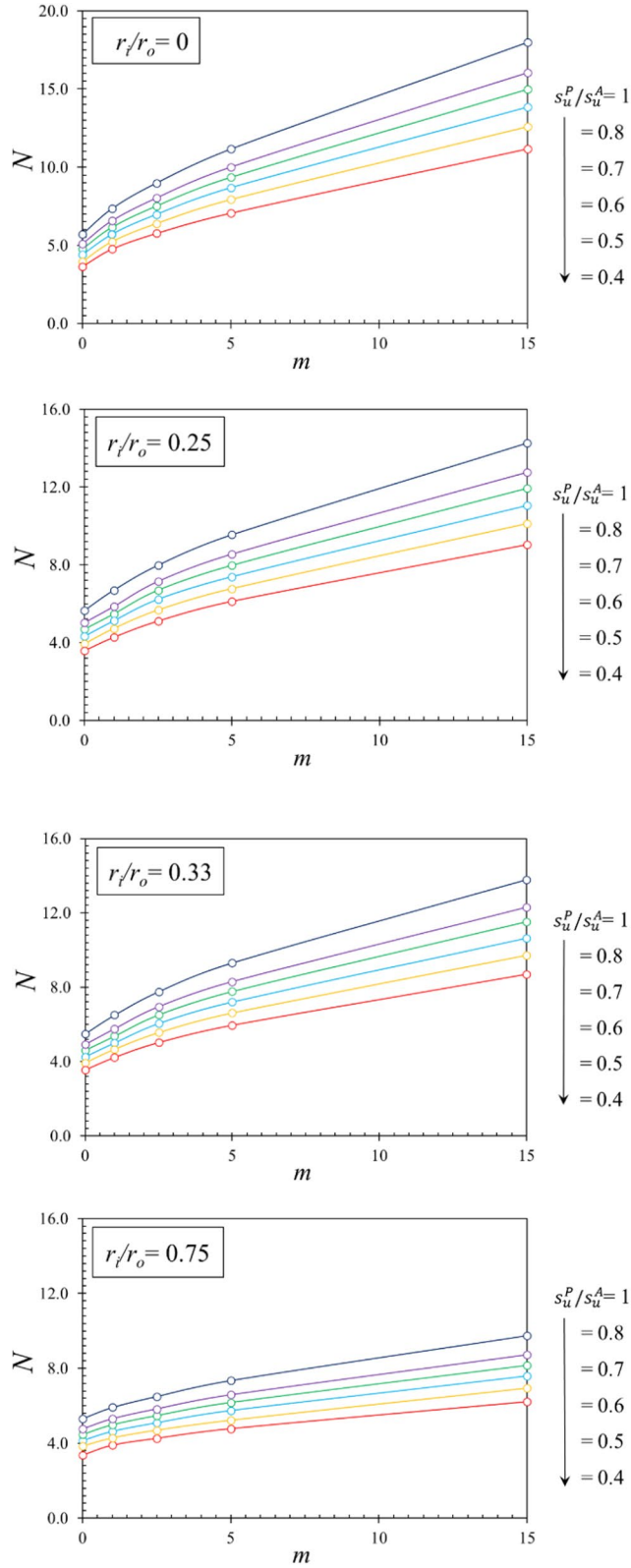


**Fig. 6** Effect of increasing strength gradient ratio ($m$) on the bearing capacity factor $N$

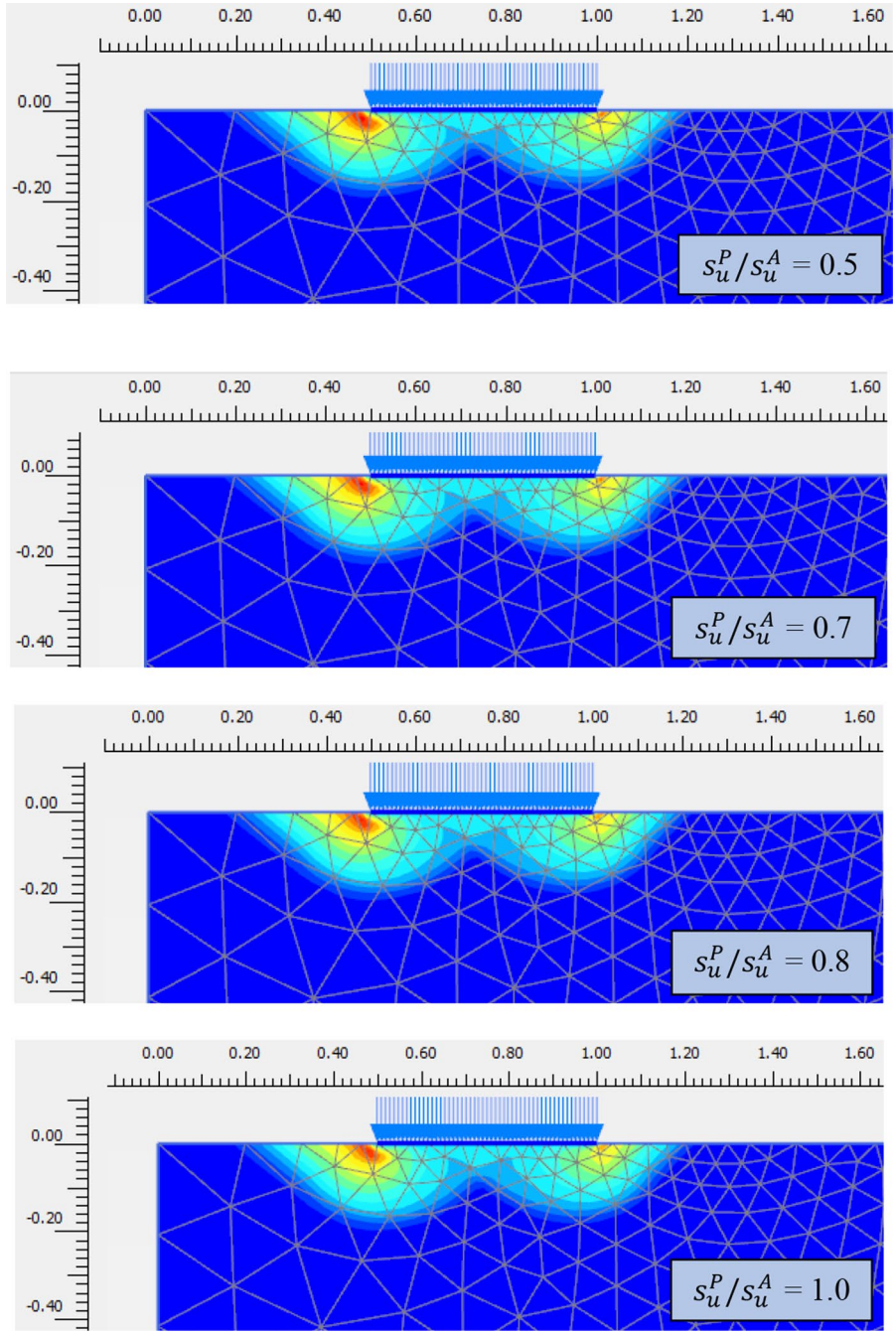


**Fig. 7** Potential failure mechanisms for the various $s_u^P/s_u^A$ ($m=5$; $r_f/r_o=0.5$)

horizontal wall displacement of braced excavation in cohesive soil. With five input parameters, the normalized maximum wall deflection was determined using the empirical equation generated by the MARS model. Other applications of the MARS model in geotechnical engineering are seen in the works of Zhou et al. (2021), Zhang et al. (2018), Zheng et al. (2019, 2020). Below is a brief description of the MARS model. More details can be found in Zhang (2019).

In the MARS model, the different splines are connected using a knot representing the end of one spline and the beginning of another. The fitted basic functions (BFs) have better flexibility to the studied model

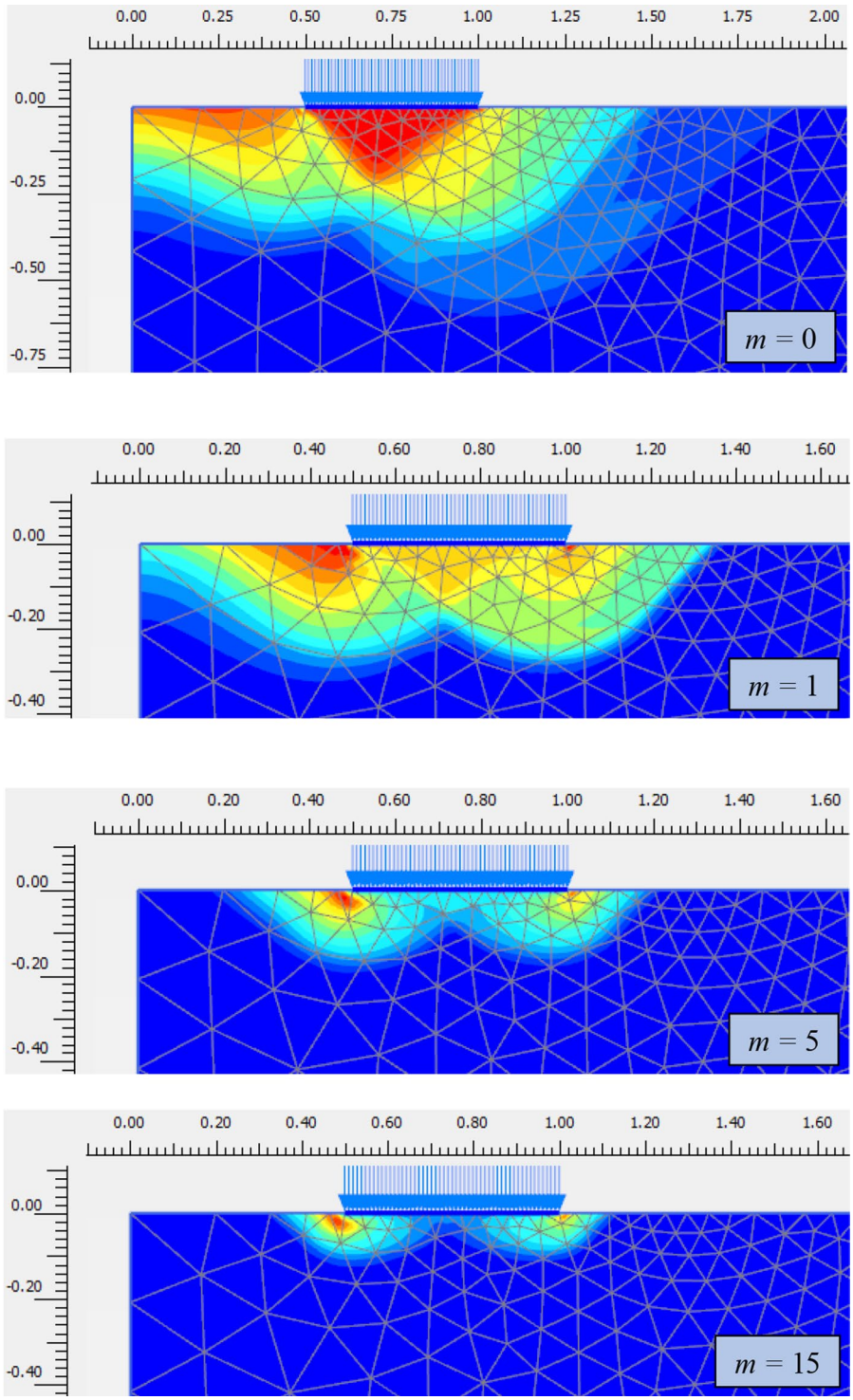


**Fig. 8** Potential failure mechanisms for the various $m$ ($s_u^P/s_u^A = 0.5$; $r_i/r_o = 0.5$)

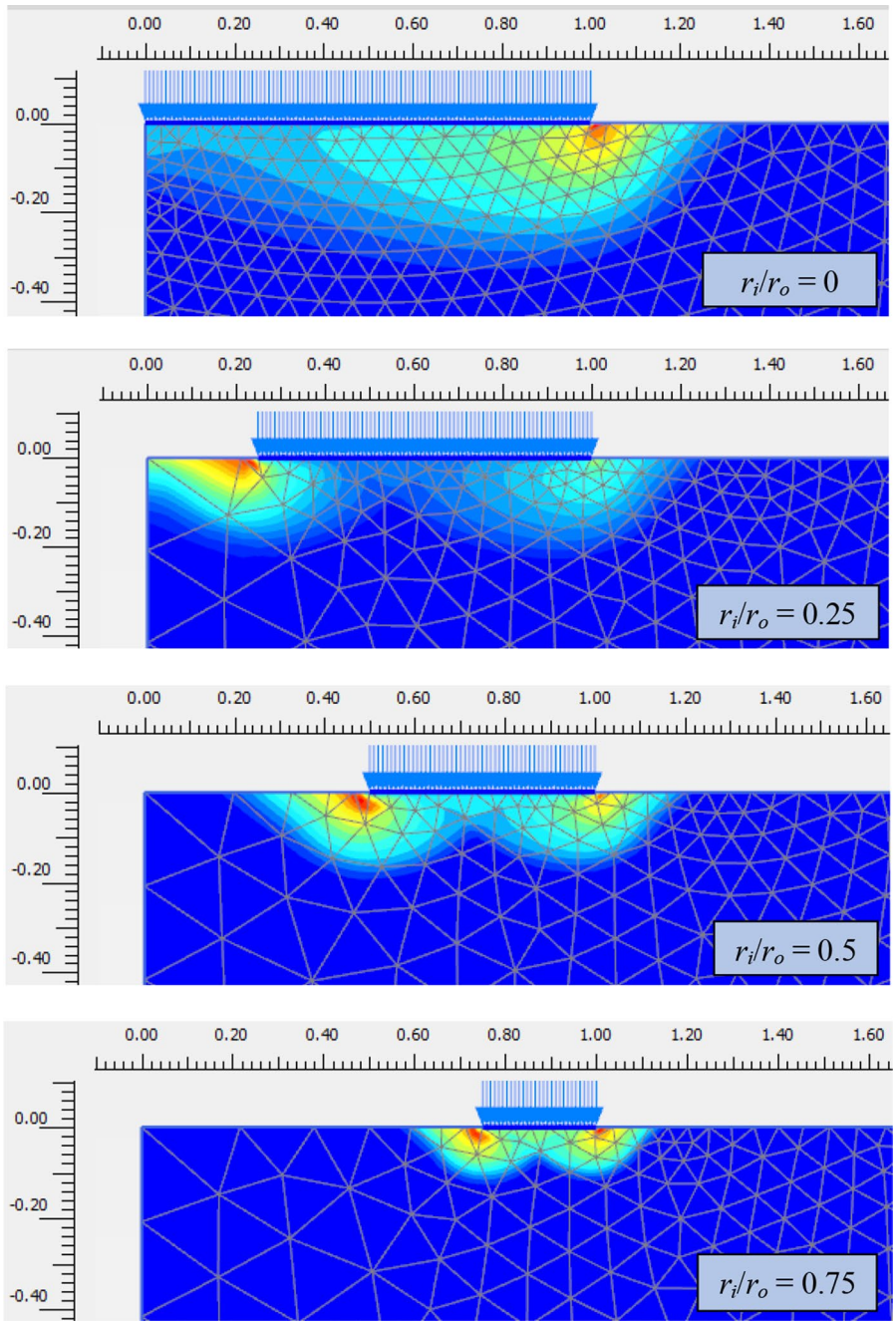


**Fig. 9** Potential failure mechanisms for the various $r_i/r_o$ ($s_u^P/s_u^A = 0.5$; $m = 5$)

where the bends, thresholds, and other derivations from linear functions are allowed (Zhang, 2019). The basic function can be written as:

$$\mathrm{BF} = \max(0,\ x - t) = \begin{cases} x - t & \text{if } x > t \\ 0 & \text{otherwise} \end{cases} \tag{5}$$

where $x$ is an input variable, and $t$ is a threshold value.

MARS model produces BFs by searching in a stepwise process, of which the knot locations are automatically determined using the adaptive regression algorithm. MARS model is presented by a two-step procedure. The first (or called "forward") step is to provide BFs as well as to find their potential knots

to optimize the model performance and fitting accuracy. The second (or "backward") step uses a pruning algorithm to delete the least effective terms, resulting in the generation of an optimal model used for the problem prediction. To build the correlation equation between the input and output variables, the MARS model combines all linear basic functions (BFs) which are described in Eq. (6), where $a_0$ is the constant, $N$ is the number of BFs, $g_n$ is the $n$th BF, $a_n$ is the coefficient of $g_n$. Note that increasing the number of basic functions can increase the accuracy of the MARS model.

$$f(x) = a_o + \sum_{n=1}^{N} a_n g_n(X). \tag{6}$$

The current study uses the MARS model to investigate sensitivity analyses of each input variables (i.e., $r_i/r_0$, $s_u^P/s_u^A$ and $m$). The aim is to build a mathematical equation for predicting the $N$ value, considering all effects of input variables. A training data set in the MARS model is selected from all FEA results of bearing capacity factors $N$. The corresponding 150 design combinations and input parameters are shown in Table 1.

To achieve the best accuracy, the chosen number of basic functions is varied to check the performance of MARS using two criteria of statistical analyses named Mean Squared Error (MSE) and the coefficient of determination ($R^2$ value). MSE represents the mean square error between the predicted output variables and the real output results. The lower MSE value, the better model can be obtained. The closer the value of $R^2$ is to 1, the better the linear regression fits the data. $R^2$ value equals 0.0 means that the model fails to predict real value, whilst 1.0 means that the forecast model is highly reliable.

Shown in Fig. 10, is the variation of MSE and $R^2$ due to the changes in the number of basic functions. Noting that the MSE decreases sharply as the

**Table 1** Bearing capacity factors $N$ of ring foundation on anisotropic and heterogeneous clays

| $m=\rho r_o/s_{u0}^A$ | $r_i/r_o$ | $s_u^P/s_u^A=0.4$ | $s_u^P/s_u^A=0.5$ | $s_u^P/s_u^A=0.6$ | $s_u^P/s_u^A=0.7$ | $s_u^P s_u^A=0.8$ | $s_u^P/s_u^A=1$ |
|---|---|---|---|---|---|---|---|
| 0 | 0 | 3.649 | 3.966 | 4.403 | 4.769 | 5.087 | 5.707 |
| | 0.25 | 3.584 | 3.941 | 4.330 | 4.694 | 5.020 | 5.643 |
| | 0.33 | 3.558 | 3.936 | 4.260 | 4.615 | 4.914 | 5.503 |
| | 0.5 | 3.558 | 3.922 | 4.229 | 4.574 | 4.857 | 5.418 |
| | 0.75 | 3.538 | 3.845 | 4.151 | 4.463 | 4.763 | 5.318 |
| 1 | 0 | 4.767 | 5.239 | 5.707 | 6.158 | 6.576 | 7.355 |
| | 0.25 | 4.280 | 4.731 | 5.127 | 5.481 | 5.849 | 6.694 |
| | 0.33 | 4.225 | 4.667 | 5.012 | 5.379 | 5.757 | 6.502 |
| | 0.5 | 4.080 | 4.466 | 4.807 | 5.152 | 5.540 | 6.339 |
| | 0.75 | 3.898 | 4.279 | 4.638 | 4.979 | 5.303 | 5.914 |
| 2.5 | 0 | 5.766 | 6.397 | 6.980 | 7.523 | 8.031 | 8.985 |
| | 0.25 | 5.113 | 5.676 | 6.232 | 6.698 | 7.147 | 7.982 |
| | 0.33 | 5.029 | 5.56 | 6.053 | 6.514 | 6.951 | 7.762 |
| | 0.5 | 4.684 | 5.171 | 5.625 | 6.051 | 6.454 | 7.205 |
| | 0.75 | 4.266 | 4.694 | 5.094 | 5.472 | 5.831 | 6.504 |
| 5 | 0 | 7.070 | 7.924 | 8.676 | 9.356 | 10.012 | 11.154 |
| | 0.25 | 6.124 | 6.776 | 7.396 | 7.974 | 8.544 | 9.548 |
| | 0.33 | 5.956 | 6.61 | 7.212 | 7.772 | 8.300 | 9.306 |
| | 0.5 | 5.480 | 6.058 | 6.603 | 7.111 | 7.590 | 8.475 |
| | 0.75 | 4.782 | 5.224 | 5.746 | 6.180 | 6.590 | 7.352 |
| 15 | 0 | 11.176 | 12.578 | 13.840 | 14.994 | 16.060 | 17.980 |
| | 0.25 | 9.042 | 10.118 | 11.060 | 11.924 | 12.756 | 14.270 |
| | 0.33 | 8.696 | 9.71 | 10.644 | 11.516 | 12.308 | 13.768 |
| | 0.5 | 7.758 | 8.656 | 9.478 | 10.234 | 10.938 | 12.226 |
| | 0.75 | 6.228 | 6.95 | 7.592 | 8.174 | 8.722 | 9.742 |

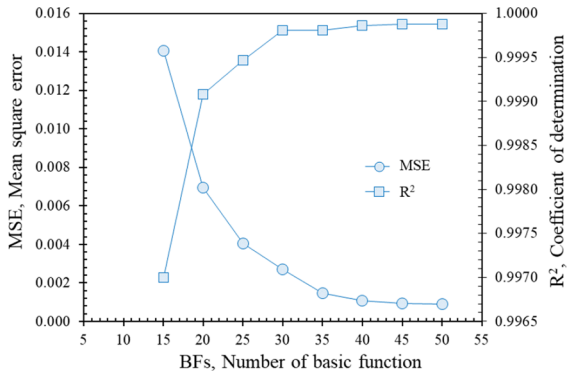


**Fig. 10** Effect of number basic functions on mean square error (MSE) and $R^2$

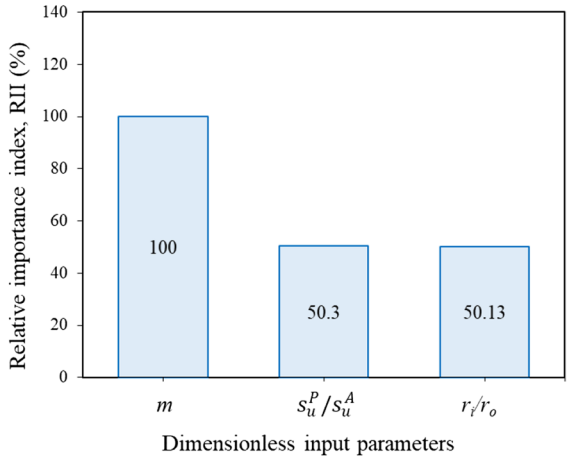


**Fig. 11** RII of dimensionless input parameters

number of BFs increases from 0 to 35, and it becomes constant for BFs > 35, though small. In contrast, the $R^2$ increases dramatically when the number of BFs increases from 0 to 30. $R^2$ becomes a constant (close to unity) for BFs > 30. It was decided that the number of BFs be chosen as 40 to perform sensitivity analyses as well as to generate the equation.

The sensitivity of each input variable is described by the relative important index (RII), as shown in Fig. 11. The value of RII indicates the weight of impaction. RII of 100% means that the respective input variable has the most important influence on the output results. This is shown for the increasing shear strength gradient ratio ($m$) in this study. The increasing shear gradient ratio has the most significant influence on the bearing capacity factor $N$. This is followed by the anisotropic ratio ($s_u^P/s_u^A$), and the ratio of inner and outer radius ($r_i/r_0$) with RII of 50.30% and 50.13% respectively. This finding has suggested that all the three investigated parameters play an important role in the design of ring foundations considering the anisotropic and heterogeneous behavior of cohesive soil.

Table 2 shows the basic functions and the mathematical equation generated by the MARS model. They can be written as Eq. (7).

$$\begin{aligned} N = {} & 5.15022 + (0.396987 \times BF1) - (0.612179 \times BF2) \\ & + (6.63818 \times BF4) - (3.39152 \times BF5) + (0.880725 \times BF6) \\ & + (0.279897 \times BF7) - (0.502764 \times BF8) + (0.546778 \times BF9) \\ & - (1.81835 \times BF11) + (1.3041 \times BF12) - (0.358855 \times BF13) \\ & - (0.288788 \times BF15) + (0.298502 \times BF16) - (0.0912928 \times BF17) \\ & + (0.757031 \times BF19) + (0.753439 \times BF22) - (1.16673 \times BF23) \\ & - (0.0754891 \times BF24) - (0.889161 \times BF26) - (0.418242 \times BF29) \\ & - (0.433821 \times BF32) - (1.31187 \times BF33) - (0.0942285 \times BF35) \\ & + (0.83858 \times BF36) + (0.225789 \times BF39) \end{aligned} \tag{7}$$

To verify the proposed Eq. (7), a comparison between the bearing capacity factors $N$ from FEA results and those from equation prediction is presented in Fig. 12. Numerical results have shown that the predicted $N$ has an excellent fit to those from FEA—with the high value of $R^2 = 99.99\%$. It can be concluded that Eq. (7) is an effective tool to estimate the bearing capacity of ring footings rest on anisotropic and heterogeneous clay.

## 5 Conclusion

Axisymmetric solutions for the bearing capacity of ring foundation resting on anisotropic and heterogenous clays have been successfully investigated in this paper using Plaxis finite element analysis and the NGI-ADP soil model—a widely used anisotropic soil model. The influences of inner and outer radius ratio ($r_i/r_0$), anisotropic ratio ($s_u^P/s_u^A$) and the shear strength gradient ratio ($m$) on the bearing capacity factor ($N$) and the failure mechanism of ring footings resting on anisotropic and heterogeneous clay are determined. The following conclusions are drawn based on the study results.

**Table 2** Basic functions and the proposed equation for the determination of $N$

| BF | Equation | BF | Equation |
|---|---|---|---|
| BF1 | max [0, ($m$ – 2.5)] | BF19 | max [0, ($m$ – 0)]×BF12 |
| BF2 | max [0, (2.5 – $m$)] | BF20 | max [0, ($m$ – 1)]×BF4 |
| BF4 | max [0, ($r_e$ – 0.4)] | BF22 | max [0, ($r_e$ – 0.6)]×BF19 |
| BF5 | max [0, ($r_i/r_o$ – 0.25)]×BF4 | BF23 | max [0, (0.6 – $r_e$)]×BF19 |
| BF6 | max [0, (0.25 – $r_i/r_o$)]×BF4 | BF24 | max [0, ($m$ – 5)] |
| BF7 | max [0, ($m$ – 5)]×BF4 | BF26 | max [0, (re – 0.6)]×BF19 |
| BF8 | max [0, (5 – $m$)]×BF4 | BF27 | max [0, (0.6 – re)]×BF19 |
| BF9 | max [0, ($r_i/r_o$ – 0.25)]×BF8 | BF29 | max [0, (0.33 – $r_i$/$ro$)]×BF20 |
| BF11 | max [0, ($r_i/r_o$ – 0.25)] | BF31 | max [0, (1 – $m$)] |
| BF12 | max [0, (0.25 – $r_i/r_o$)]×BF4 | BF32 | max [0, ($r_i/r_o$ – 0.33)]×BF31 |
| BF13 | max [0, ($m$ – 2.5)]×BF11 | BF33 | max [0, (0.33 – $r_i/r_o$)]×BF31 |
| BF15 | max [0, ($r_i/r_o$ – 0.5)]×BF7 | BF35 | max [0, (0.5 – $r_i/r_o$)]×BF24 |
| BF16 | max [0, (0.5 – $r_i/r_o$)]×BF7 | BF36 | max [0, ($r_i/r_o$ – 0.33)]×BF2 |
| BF17 | max [0, (2.5 – $m$)]×BF5 | BF39 | max [0, (2.5 – $m$)]×BF27 |

$N$ = 5.15022 + (0.396987×BF1) – (0.612179×BF2) + (6.63818×BF4) – (3.39152×BF5) + (0.880725×BF6) + (0.279897×BF7) – (0.502764×BF8) + (0.546778×BF9) – (1.81835×BF11) + (1.3041×BF12) – (0.358855×BF13) – (0.288788×BF15) + (0.298502×BF16) – (0.0912928×BF17) + (0.757031×BF19) + (0.753439×BF22) – (1.16673×BF23) – (0.0754891×BF24) – (0.889161×BF26) – (0.418242×BF29) – (0.433821×BF32) – (1.31187×BF33) – (0.0942285×BF35) + (0.83858×BF36) + (0.225789×BF39)

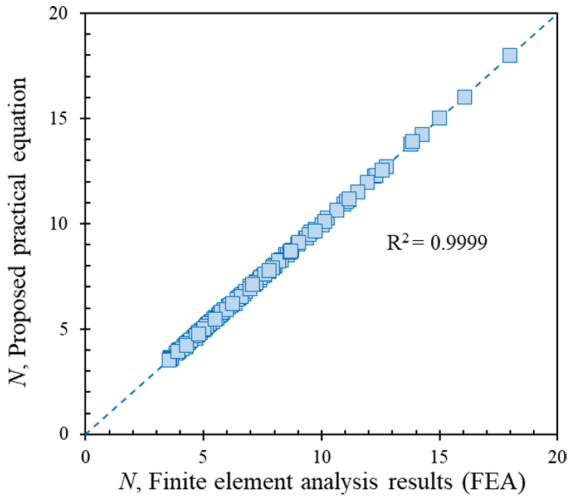


**Fig. 12** Comparison of results—the finite element analysis results (Plaxis) and the proposed equation

- FEA results have shown that the bearing capacity factor $N$ decreases with the increasing inner and outer radius ratio ($r_i/r_0$) and the decreasing anisotropic ratio ($s_u^P/s_u^A$). In contrast, the bearing capacity factor $N$ increases with the increasing shear strength gradient ratio ($m$).
- Using the MARS model for sensitive analysis of each parameter, it was concluded that the increasing shear gradient ratio ($m$) is the most influential parameter with a relative importance index RII = 100%. This is followed by the anisotropic ratio ($s_u^P/s_u^A$) and ratio of inner and outer radius ($r_i/r_0$) with RII = 50.30 and 50.13%, respectively.
- An accurate equation is proposed with $R^2$ = 99.99%, which is considered as an effective tool for engineering practitioners to evaluate the bearing capacity of ring foundations in anisotropic and heterogenous clays. Note that the value of is the highest accuracy MARS models can provide according to some previous works (Lai et al. 2021a, b) Zhang et al. 2017, 2018, 2019, 2020; Zhou et al. 2021).

**Acknowledgements** We would like to thank Ho Chi Minh City University of Technology (HCMUT), VNU-HCM for the support of time and facilities for this study. We are respect Thammasat University Research Unit in Structural and Foundation Engineering, Thammasat University and University of Southern Queensland (USQ) for the contribution and support for this study.

**Funding** Open Access funding enabled and organized by CAUL and its Member Institutions.

**Data Availability Statement** All data, models, or code that support the findings of this study are available from the corresponding author upon reasonable request.

**Declarations**

**Conflict of Interest** The authors declare no conflict of interest.



## References

Aamodt MT, Grimstad G and Nordal S (2021). Effect of strength anisotropy on the stability of natural slopes. In: IOP conference series: earth and environmental science, vol 710, no 1. IOP Publishing, p 012025

Benmebarek S, Remadna MS, Benmebarek N, Belounar L (2012) Numerical evaluation of the bearing capacity factor of ring footings. Comput Geotech 44:132–138

Benmebarek S, Saifi I, Benmebarek N (2017) Undrained vertical bearing capacity factors for ring shallow footings. Geotech Geol Eng 35(1):355–364

Beygi M, Keshavarz A, Abbaspour M, Vali R, Saberian M, Li J (2020) Finite element limit analysis of the seismic bearing capacity of strip footing adjacent to excavation in c-φ soil. Geomech Geoeng 17(1):1–14

Bhattacharya P (2016) Pullout capacity of strip plate anchor in cohesive sloping ground under undrained condition. Comput Geotech 78:134–143

Bhattacharya P, Sahoo S (2017) Uplift capacity of horizontal anchor plate embedded near to the cohesionless slope by limit analysis. Geomech Eng 13(4):701–714

Bhattacharya P (2018) Undrained uplift capacity of strip plate anchor nearby clayey slope. Geotech Geol Eng 36(2):1393–1407

Birid K, Choudhury D (2021) Depth factors for ring foundations in cohesive soil using numerical analysis. Int J Geotech Eng 15(10):1–11

Brinkgreve R, Vermeer PA (2019) PLAXIS 2D reference manual CONNECT edition V20. Delft University, Delft

Chakraborty A, Goswami D (2021) Three-dimensional (3D) slope stability analysis using stability charts. Int J Geotech Eng 15(5):642–649

Chatterjee D, Murali Krishna A (2021) Stability analysis of two-layered non-homogeneous slopes. Int J Geotech Eng 15(5):617–623

Chavda JT, Dodagoudar GR (2021) On vertical bearing capacity of ring footings: finite element analysis, observations and recommendations. Int J Geotech Eng 15(10):1207–1219

Chavda JT, Dodagoudar GR (2019) Finite element evaluation of vertical bearing capacity factors $c'$, $N'c$, $N'q$, $N'\gamma$ for ring footings. Geotech Geol Eng 37(2):741–754

Choobbasti AJ, Hesami S, Najafi A, Pirzadeh S, Farrokhzad F, Zahmatkesh A (2010) Numerical evaluation of bearing capacity and settlement of ring footing; case study of Kazeroon cooling towers. Int J Res Rev Appl Sci 4:263–271

D'Ignazio M, Lansivaara T, Jostad HP (2017) Failure in anisotropic sensitive clays: a finite element study of the perni failure test. Can Geotech J 54(7):1013–1033 (**cgj-2015-0313**)

Demir A, Örnek M, Laman M, Yildiz A (2012). Analysis of ring footings using field test results. In: Proc., 3rd Int. Conf. Of New Developments in Soil Mechanics and Geotechnical Engineering, Nicosia, Northern Cyprus, pp 179–184

Gholami H, Hosseininia ES (2017) Bearing capacity factors of ring footings by using the method of characteristics. Geotech Geol Eng 35(5):2137–2146

Grimstad G, Andresen L, Jostad HP (2012) NGI-ADP: Anisotropic shear strength model for clay. Int J Numer Anal Meth Geomech 36(4):483–497

Hansen LA, Clough W (1981). The significance of clay anisotropy in finite element analysis of supported excavations. In: Proceedings of symposium of implementation of computer procedure of stress strain laws in geotechnical engineering, vol I–II, Chicago Illinois, 3–6 August

Hataf N, Razav IM (2003) Behavior of ring footings on sand. Iran J Sci Technol Trans B 27:47–56

Halder P, Manna B (2020). Performance evaluation of piled rafts in sand based on load-sharing mechanism using finite element model. Int J Geotechn Eng 1–18

Hamouma D, Messameh AA, Tallah N (2021). Probabilistic analysis of lateral bearing capacity of pile-soil system. Int J Geotechn Eng 1–7

Huynh QT, Lai VQ, Shiau J, Keawsawasvong S, Mase LZ, Tra HT (2022a) On the use of both diaphragm and secant pile walls for a basement upgrade project in Vietnam. Innov Infrastruct Solut 7(1):1–10

Huynh QT, Lai VQ, Boonyatee T, Keawsawasvong S (2022b) Verification of soil parameters of hardening soil model with small-strain stiffness for deep excavations in medium dense sand in Ho Chi Minh City, Vietnam. Innov Infrastruct Solut 7(1):1–20

Keawsawasvong S (2021). Bearing capacity of conical footings on clays considering combined effects of anisotropy and non-homogeneity. Ships Offshore Struct

Keawsawasvong S, Lai VQ (2021) End bearing capacity factor for annular foundations embedded in clay considering the effect of the adhesion factor. Int J Geosynthet Ground Eng 7(1):1–10

Keawsawasvong S, Lawongkerd J (2021) Influences of anisotropic undrained shear strengths of clays on pullout capacity of planar caissons. Sci Technol Asia 26(3):90–98

Keawsawasvong S, Shiau J, Ngamkhanong C, Lai VQ, Thongchom C (2022) Undrained stability of ring foundations: axisymmetry, anisotropy, and non-homogeneity. Int J Geomech, ASCE 22(1):04021253

Keawsawasvong S, Ukritchon B (2017a) Undrained lateral capacity of I-shaped concrete piles. Songklanakarin J Sci Technol 39(6):751–758

Keawsawasvong S, Ukritchon B (2017b) Finite element analysis of undrained stability of cantilever flood walls. Int J Geotech Eng 11(4):355–367

Keawsawasvong S, Ukritchon B (2020) Design equation for stability of shallow unlined circular tunnels in Hoek-Brown rock masses. Bull Eng Geol Env 79:4167–4190

Keawsawasvong S, Ukritchon B (2021) Undrained stability of plane strain active trapdoors in anisotropic and non-homogeneous clays. Tunnel Undergr Space Technol 107:103628

Keawsawasvong S, Yoonirundorn K, Senjuntichai T (2021) Pullout capacity factor for cylindrical suction caissons in anisotropic clays based on Anisotropic Undrained Shear failure criterion. Transp Infrastruct Geotechnol 8(4):629–644

Khatri VN, Kumar J (2009) Bearing capacity factor Nγ for a rough conical footing. Geomech Eng 1:205–218

Krabbenhoft K, Galindo-Torres SA, Zhang X, Krabbenhøft J (2019) AUS: Anisotropic undrained shear strength model for clays. Int J Numer Anal Meth Geomech 43(17):2652–2666

Kumar J, Chakraborty M (2015) Bearing capacity factors for ring foundations. J Geotech Geoenviron Eng 141:06015007

Ladd CC (1991) Stability evaluations during stage construction. J Geotechn Eng 117(4):540–615

Ladd CC, DeGroot DJ (2003). Recommended practice for soft ground site characterization. Arthur Casagrande Lecture. In: Proceedings of the 12th panamerican conference on soil mechanics and geotechnical engineering, Cambridge

Lai F, Zhang N, Liu S, Sun Y, Li Y (2021b). Ground movements induced by installation of twin large diameter deeply-buried caissons: 3D numerical modeling. Acta Geotech 1–29

Lai VQ, Nguyen DK, Banyong R, Keawsawasvong S (2021a). Limit analysis solutions for stability factor of unsupported conical slopes in clays with heterogeneity and anisotropy. Int J Comput Mater Sci Eng 2150030

Lai VQ, Banyong B, Keawsawasvong S (2022) Stability of limiting pressure behind soil gaps in contiguous pile walls in anisotropic clays. Eng Fail Anal 134:106049

Langford J, Karlsrud K, Bengtsson E, Hof C, Oscarsson R (2021) Comparison between predicted and measured performance of a deep excavation in soft clay in Gothenburg, Sweden. In: Geotechnical aspects of underground construction in soft ground: proceedings of the tenth international symposium on geotechnical aspects of underground construction in soft ground, IS-Cambridge 2022, Cambridge, UK, 27–29 June 2022. CRC Press, p 83

Lee JK, Jeong S, Lee S (2016) Undrained bearing capacity factors for ring footings in heterogeneous soil. Comput Geotech 75:103–111

Li Y, Zhang W (2020) Investigation on passive pile responses subject to adjacent tunnelling in anisotropic clay. Comput Geotech 127:103782

Li Y, Zhang W, Zhang R (2021). Numerical investigation on performance of braced excavation considering soil stress-induced anisotropy. Acta Geotech 1–13

Nguyen DK, Nguyen TP, Keawsawasvong S, Lai VQ (2021). Vertical uplift capacity of circular anchors in clay by considering anisotropy and non-homogeneity. Transp Infrastruct Geotechnol

Ohri M, Purhit D, Dubey M (1997) Behavior of ring footing on dune sand overlying dense sand. In: Proceedings of the international conference on civil engineering, Tehran, Iran, 12 August 1997, pp 22–24

Papadopoulou K, Gazetas G (2020) Shape effects on bearing capacity of footings on two-layered clay. Geotech Geol Eng 38(2):1347–1370

Pirastehfar K, Shivaei S, Sadaghiani MH, Nikooee E (2020) 3D numerical investigation of the effects of driving of the new mechanized tunnel on existing segmental linings and ground surface settlements-a case study: Shiraz metro line 2. Int J Geotech Eng 1–12

Shalaby SI (2017) Bearing capacity of ring footing on stabilized clay with sand trench-stone pile combination. Int J Sci Eng Appl Sci 3(5):218–226

Shiau J, Yu H (2000) Shakedown analysis of flexible pavements. In: Smith DW, Carter JP (eds) Proc. of the John Booker memorial symposium, pp 643–653

Shiau J, Smith C (2006a) Numerical analysis of passive earth pressures with interfaces. In: Proceedings of the III European conference on computational mechanics (ECCM 2006), 5–8 June 2006, Lisbon, Portugal

Shiau J, Lyamin AV, Sloan SW (2006b) Application of pseudo-static limit analysis in geotechnical earthquake design. In: 6th European conference on numerical methods in geotechnical eng.: Graz, Austria

Shiau J, Pather S, Ayers R (2006c) Developing physical models for geotechnical teaching and research. In: Proc. 6th IC physical modelling in geotechnics, pp 157–162

Shiau JS, Watson JF (2008) 3D bearing capacity of shallow foundations located near deep excavation sites. In: 2008 international conference on deep excavation: challenges risk management of underground construction (ICDE 2008), 10–12 Nov 2008, Singapore

Shiau JS, Sams MS, Zhang J, Kemp RJ (2014) Settlement analyses of underground circular tunneling in soft clay, In: Geotechnical aspects of underground construction in soft ground. Taylor & Francis (CRC Press), pp 347–352

Shiau J, Lamb B, Sams M (2016a) The use of sinkhole models in advanced geotechnical engineering teaching. Int J Geomate 10(2):1718–1724

Shiau J, Sams M, Lamb B (2016b) Introducing advanced topics in geotechnical engineering teaching–tunnel modelling. Int J Geomate 10(1):1698–1705

Shiau J, Sams M, Lamb B, Lobwein J (2017) Stability charts for unsupported circular tunnels in cohesive soils. Int J of GEOMATE 13(39):95–102

Shiau J, Al-Asadi F (2020a) Three-dimensional analysis of circular tunnel headings using Broms and Bennermark's original stability number. Int J Geomech 20(7):06020015
Shiau J, Al-Asadi F (2020b) Three-dimensional heading stability of twin circular tunnels. Geotech Geol Eng 38(3):2973–2988
Shiau J, Al-Asadi F (2020c) Stability analysis of twin circular tunnels using shear strength reduction method. Géotech Lett 10(2):311–319
Shiau J, Al-Asadi F (2020d) Twin tunnels stability factors Fc, Fs and Fr. Geotech Geol Eng. https://doi.org/10.1007/s10706-020-01495-z
Shiau J, Al-Asadi F (2021) Revisiting circular tunnel stability using Broms and Bennermarks' original stability number. Int J Geomech 21(5):06021009
Shiau J, Lee JS, Al-Asadi F (2021) Three-dimensional stability analysis of active and passive trapdoors. Tunnel Undergr Space Technol 107:103635
Tho KK, Chen Z, Leung CF, Chow YK (2014) Pullout behaviour of plate anchor in clay with linearly increasing strength. Can Geotech J 51(1):92–102
Ukritchon B, Boonyatee T (2015) Soil parameter optimization of the NGI-ADP constitutive model for Bangkok soft clay. Geotech Eng 46(1):28–36
Ukritchon B, Keawsawasvong S, Yingchaloenkitkhajorn K (2017a) Undrained face stability of tunnels in Bangkok subsoils. Int J Geotech Eng 11(3):262–277
Ukritchon B, Keawsawasvong S (2017) Error in Ito and Matsui's limit equilibrium solution of lateral force on a row of stabilizing piles. J Geotech Geoenviron Eng, ASCE 143(9):02817004
Ukritchon B, Keawsawasvong S (2019) Design equations of uplift capacity of circular piles in sands. Appl Ocean Res 90:101844
Ukritchon B, Keawsawasvong S (2020) Undrained lower bound solutions for end bearing capacity of shallow circular piles in non-homogeneous and anisotropic clays. Int J Numer Anal Meth Geomech 44(5):596–632
Ukritchon B, Wongtoythong P, Keawsawasvong S (2018) New design equation for undrained pullout capacity of suction caissons considering combined effects of caisson aspect ratio, adhesion factor at interface, and linearly increasing strength. Appl Ocean Res 75:1–14
Ukritchon B, Yingchaloenkitkhajorn K, Keawsawasvong S (2017b) Three-dimensional undrained tunnel face stability in clay with a linearly increasing shear strength with depth. Comput Geotech 88:146–151
Ukritchon B, Yoang S, Keawsawasvong S (2019) Three-dimensional stability analysis of the collapse pressure on flexible pavements over rectangular trapdoors. Transp Geotech 21:100277
Ukritchon B, Yoang S, Keawsawasvong S (2020) Undrained stability of unsupported rectangular excavations in non-homogeneous clays. Comput Geotech 117:103281
Yang C, Zhu Z, Xiao Y (2020) Bearing capacity of ring foundations on sand overlying clay. Appl Sci 10(13):4675
Yodsomjai W, Keawsawasvong S, Lai VQ (2021a) Limit analysis solutions for bearing capacity of ring foundations on rocks using Hoek-Brown failure criterion. Int J Geosynthet Gr Eng 7(2):1–10
Yodsomjai W, Keawsawasvong S, Senjuntichai T (2021b) Undrained stability of unsupported conical slopes in anisotropic clays based on Anisotropic Undrained Shear failure criterion. Transp Infrastruct Geotechnol 8(4):557–568
Yodsomjai W, Keawsawasvong S, Likitlersuang S (2021c) Stability of unsupported conical slopes in Hoek-Brown rock masses. Transp Infrastruct Geotechnol 8:278–295
Yu HS, Sloan SW (1994) Limit analysis of anisotropic soils using finite elements and linear programming. Mech Res Commun 21(6):545–554
Zhang W, Zhang R, Goh ATC (2018) MARS inverse analysis of 954 soil and wall properties for braced excavations in clays. Geomech Eng 16(6):577–588
Zhang W (2019) MARS applications in geotechnical engineering systems. Springer, Beijing
Zhang W, Zhang Y, Goh ATC (2017) Multivariate adaptive regression splines for inverse analysis of soil and wall properties in braced excavation. Tunn Undergr Sp Tech 64:24–33
Zhang R, Chongzhi Wu, Goh ATC, Böhlke T, Zhang W (2021) Estimation of diaphragm wall deflections for deep braced excavation in anisotropic clays using ensemble learning. Geosci Front 12(1):365–373
Zhang W, Li Y, Wu C, Li H, Goh ATC, Liu H (2020) Prediction of lining response for twin tunnels constructed in anisotropic clay using machine learning techniques. Undergr Space
Zhao L, Wang JH (2008) Vertical bearing capacity for ring footings. Comput Geotech 35:292–304
Zheng G, Yang P, Zhou H, Zeng C, Yang X, He X, Yu X (2019) Evaluation of the earthquake induced uplift displacement of tunnels using multivariate adaptive regression splines. Comput Geotech 113:103099
Zheng G, Zhang W, Zhou H, Yang P (2020) Multivariate adaptive regression splines model for prediction of the liquefaction-induced settlement of shallow foundations. Soil Dyn Earthq Eng 132:106097
Zhou H, Xu H, Yu X, Guo Z, Zheng G, Yang X (2021) Evaluation of the bending failure of columns under an embankment loading. Int J Geomech 21(7):04021112